ACS APPLIED MATERIALS & INTERFACES

www.acsami.org

Research Article

Selective Anticancer Materials by Self-Assembly of Synthetic Amphiphiles Based on *N*-Acetylneuraminic Acid

Jiwon Hwang, Ye Rim Kim, Jung Yeon Park, Woo Hyun Nam, Jehan Kim, Jinhan Cho, and Yongju Kim*

Cite This: *ACS Appl. Mater. Interfaces* 2022, 14, 16100−16107

Read Online

ACCESS | Metrics & More | Article Recommendations | Supporting Information

ABSTRACT: *N*-Acetylneuraminic acid (Neu5Ac), one of the abundant types of sialic acid, is an emerging anticancer agent owing to its ability to target selectins in the plasma membrane of cancer cells. Considering the functionality of Neu5Ac, obtaining novel Neu5Ac-conjugated materials with a selective and an enhanced antitumor activity has remained a challenge. Herein, we report the supramolecular materials of three novel amphiphiles composed of Neu5Ac as a hydrophilic segment and pyrene or adamantane as a hydrophobic segment. The synthetic amphiphiles **1**, **2**, and **3** self-assembled into ribbons, vesicles, and irregular aggregates in an aqueous solution, respectively. Among the materials, vesicles of amphiphile **2** showed the most substantial selectivity toward cancer cells, followed by cell death due to the production of reactive oxygen species by the pyrene group. The dual advantage of Neu5Ac-selectivity and the pyrene-cytotoxicity of vesicles of amphiphile **2** can provide a strategy for effective anticancer materials.

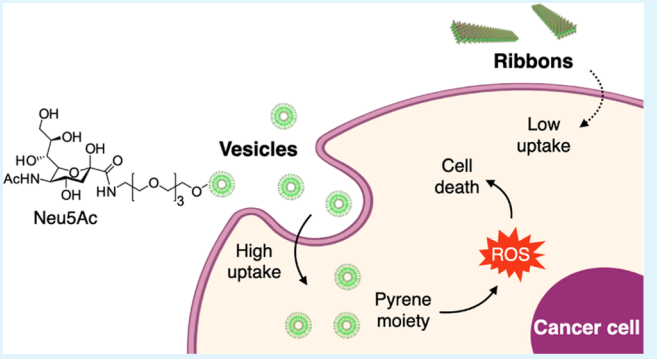

KEYWORDS: *supramolecular materials, anticancer materials, sialic acid, N-acetylneuraminic acid, Neu5Ac, active targeting cancer therapy, reactive oxygen species*

1. INTRODUCTION

Sialic acid (SA) is a generic term for more than 50 derivatives of neuraminic acid having the nine-carbon backbone.[1] *N*-Acetylneuraminic acid (Neu5Ac), one of the most abundant SAs, is located in the glycan chain terminal on the cell surface in vertebrates.[2,3] Consequently, Neu5Ac participates in trafficking, cell−cell interactions, and cell−extracellular matrix interactions.[4] Therefore, Neu5Ac plays important physiological and pathological roles in processes such as the progression and spread of tumors.[5] Several applications based on the function of Neu5Ac have been reported in anti-adhesive systems, drug delivery systems, antiviral materials, and cancer treatments.[6] A novel material based on the functionality of Neu5Ac, such as anthraquinone-SA, has been reported.[7] In addition, Neu5Ac-based systems such as selenium nanoparticles[8] and pixantrone-loaded liposomes[9] showed binding ability to the selectins in the plasma membrane of cancer cells, resulting in a selective antitumor effect. Despite the ability of Neu5Ac derivatives to specifically target cancer cells, the development and applications of Neu5Ac-based anticancer materials are challenging because of the limited antitumor activity and synthetic complexities of Neu5Ac derivatives.[10,11] Besides, the relationship between Neu5Ac-conjugated architectures and their activity has not been reported.

Supramolecular materials are a convenient toolkit for constructing unique structures based on non-covalent bonds such as hydrophobic interactions, hydrogen bonds, van der Waals forces, and $\pi-\pi$ interactions.[12,13] For example, various structures such as fibers,[14] tubules,[15] toroids,[16] ribbons,[17] sheets,[18] and vesicles[19] using the supramolecular approach have been reported. Many synthetic supramolecular systems bind to biological targets at the nanoscale level through multivalent binding interactions.[20] Moreover, supramolecular materials with a selective binding ability have been used as antimicrobial agents, biosensors, drug release vehicles, and cell stimulators.[21] Therefore, diverse nanostructures using the supramolecular approach can provide a novel strategy for biological applications of Neu5Ac-conjugated materials at the nanoscopic level.

Here, we report the different supramolecular structures of three Neu5Ac-based amphiphiles **1**, **2**, and **3** prepared by simple synthetic methods (Schemes 1, 2, and 3). Hydrophobic aromatic pyrene was connected to Neu5Ac with linkers having different lengths using an amide bond to synthesize amphiphiles **1** and **2**. Adamantane was used as a hydrophobic

Received: February 16, 2022
Accepted: March 18, 2022
Published: April 4, 2022

https://doi.org/10.1021/acsami.2c02922
ACS Appl. Mater. Interfaces 2022, 14, 16100−16107

Scheme 1. Synthesis Scheme of Molecules 1, 2, and 3

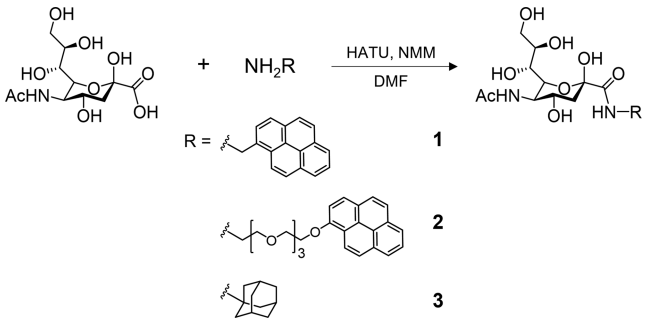

rigid segment to produce amphiphile **3**. The supramolecular structures of amphiphiles **1**, **2**, and **3** were characterized as ribbons, vesicles, and irregular aggregates, respectively, with Neu5Ac exposed on their surfaces. The Neu5Ac-selectivity and pyrene-cytotoxicity of the materials were investigated between the different supramolecular structures. The vesicles of amphiphile **2** showed a considerable selectivity toward the cancer cell (HeLa cell) rather than normal cell (HEK293), followed by cell death due to the production of reactive oxygen species (ROS) by the pyrene group.

2. RESULTS AND DISCUSSION

2.1. Self-Assembled Structures of Amphiphiles 1, 2, and 3. The amphiphilic supramolecular monomers were constructed by connecting the hydrophilic Neu5Ac and hydrophobic pyrene or adamantane using an amide bond with different lengths of linkers (Figure 1a; see also Figures S1−S4). The aggregation behavior of molecule **1** was initially investigated using UV−visible spectroscopy and fluorescence spectroscopy. When the concentration of amphiphile **1** was increased, the absorption coefficient and the fluorescence intensity decreased, indicating an aromatic interaction of the pyrene group of **1** (see Figure S5). The structural analysis of the supramolecular material was performed using negatively stained transmission electron microscopy (TEM), and the image showed that amphiphile **1** in aqueous solution self-assembled into 1 μm-wide rigid ribbons (Figure 2a). The ribbon structures were analyzed using fluorescence optical microscopy (FOM), which proved that the ribbons were formed in the solution phase (Figure 2b). The ribbon structure was also corroborated using atomic force microscopy (AFM) and scanning electron microscopy (SEM), which are consistent with TEM and FOM images (see Figures S6 and S7). The packing arrangement of pyrene groups of amphiphile **1** was analyzed by proton NMR measurement using solvents with different ratios of methanol-d_4 (CD_3OD) and deuterium oxide (D_2O) (Figure 2c). The NMR peaks of pyrene are denoted by different shapes according to the corresponding protons; dot (●), triangle (▲), and square (■). The spectra showed that most pyrene peaks were shifted to downfield when the ratio of D_2O was gradually increased, indicating that the assembly of pyrene units occurred *via* $\pi-\pi$ interaction.[22] In contrast, the H10 peak of pyrene was moved upfield from 8.39 to 8.33 ppm. Density functional theory (DFT)-based proton NMR prediction of *N*-(1-pyrenylmethyl)acetamide was performed to investigate the peak shift of H10 (see Figure S8). The calculated chemical shift of H10 of different conformers increased from 8.13 to 8.83 ppm as the oxygen of the amide bond moved close to H10 and decreased the electron density of H10. Molecular simulation using the tetramer of amphiphile **1** indicated that pyrene groups in the aggregates are likely to be oriented perpendicular to the plane of the ribbon, and Neu5Ac is exposed on the surface of the ribbons. The simulation results also showed that water bridges between the amide bonds of Neu5Ac segments were adopted to form the stable aggregates. Taken together, the water bridges induced the specific conformer of amphiphile **1**, in which the amide bond rotated in the opposite side of H10, leading to a decrease in the chemical shift. A small-angle X-ray scattering (SAXS) measurement was performed to investigate the packing arrangement of the ribbons. The SAXS result exhibited a pattern with d = 2.9 nm, which is in good agreement with the length of dimer **1** calculated by the DFT calculation (Figure 2d,e).

Amphiphile **2** consists of Neu5Ac and pyrene, conjugated with tetraethylene glycol as a long linker to provide supramolecular structural diversity through increased solubility and flexibility. The fluorescence intensity at 387 nm was quenched in a concentration-dependent manner, implying the self-assembly of amphiphile **2** (see Figure S9). With respect to peak I, the relatively lower peak intensity of II in the emission spectrum of **2** than that of **1** was characteristic toward pyrene monomers (Figure 3a).[23] A considerably weak intensity of **2** near 500 nm indicated that the packing of amphiphile **2** was looser than that of **1**, demonstrating a negligible amount of pyrene as dimers in the excited state (excimers).[24] The self-assembling behavior of amphiphile **2** was further studied using a dynamic light scattering experiment that exhibited an average value of 150 nm (Figure 3b). This value is consistent with the diameter of spherical aggregates acquired from the TEM image (Figure 3c). The self-assembled spherical structures of amphiphile **2** were also observed using AFM and SEM (Figure 3d and 3e). The FOM image revealed that the self-assembled spheres of amphiphile **2** could be formed in the solution phase (see Figure S10). To corroborate the structural details of the spherical aggregates, a dye encapsulation experiment was performed. The results showed peaks corresponding to the aggregate of amphiphile **2** and the pyranine dye after removing the free pyranine from the aggregates using a Sephadex column, indicating that the spherical aggregates of amphiphile **2** are vesicular structures with hydrophilic pyranine dye inside them (see Figure S11). The packing arrangement of

Scheme 2. Synthetic Method of a Hydrophobic Segment of Molecule 1

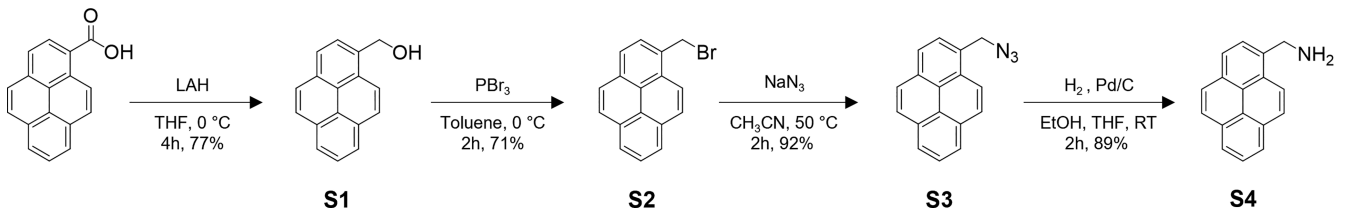

https://doi.org/10.1021/acsami.2c02922
ACS Appl. Mater. Interfaces 2022, 14, 16100−16107

Scheme 3. Synthetic Method of a Hydrophobic Segment of Molecule 2

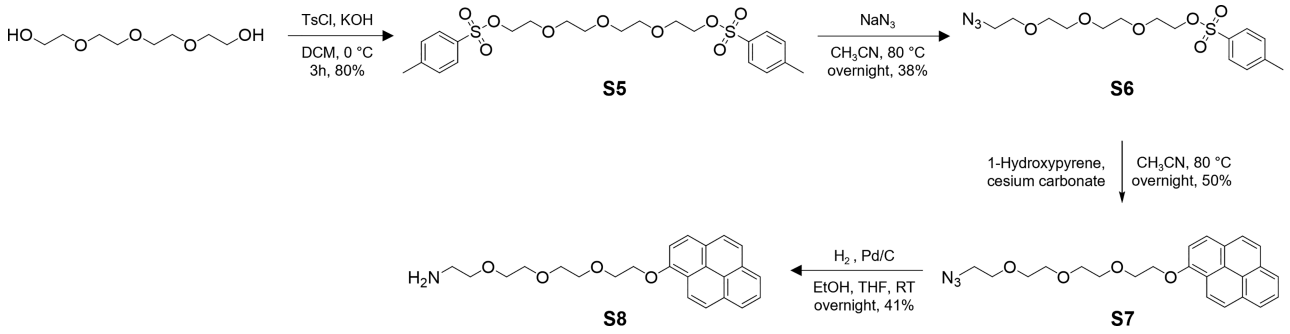

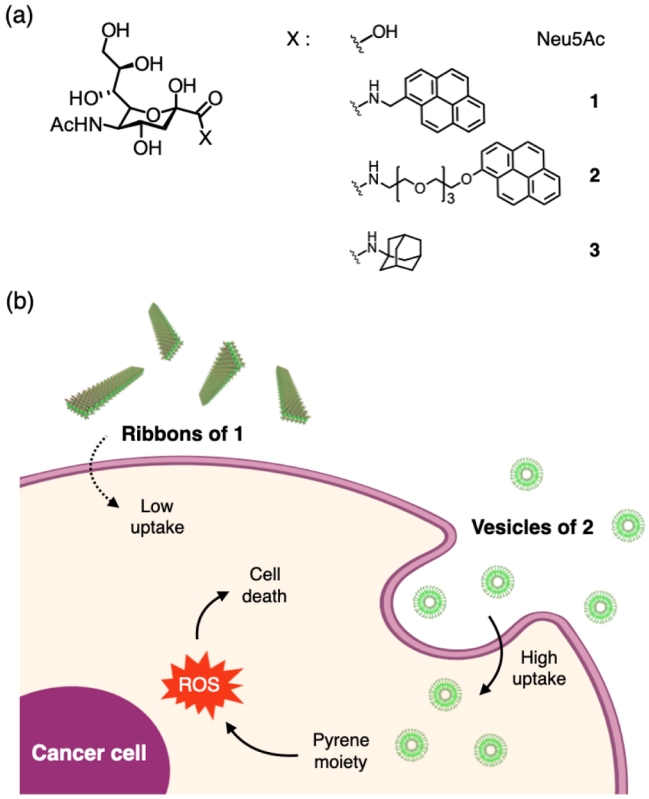

Figure 1. (a) Chemical structures of Neu5Ac and amphiphiles **1**, **2**, and **3**. (b) Schematic representation of Neu5Ac-based supramolecular materials for anticancer therapy.

amphiphile **2** was simulated after energy minimization using DFT calculation (B3LYP-D3, 6-31G**), which showed a dimer with a length of 3.8 nm (Figure 3f; see also Figure S12). However, the vesicles of amphiphile **2** did not show any SAXS patterns because of the absence of highly ordered packing (see Figure S13).

Amphiphile **3** with an adamantane as a hydrophobic rigid aliphatic segment instead of a flat aromatic ring was also synthesized to investigate the role of aromatic interactions during molecular assembly. Amphiphile **3** did not show any specific absorbance or fluorescence because of the lack of a chromophore. The negatively stained TEM image showed irregular aggregates, and no SAXS patterns were observed (see Figure S14). These results imply that polycyclic aromatic hydrocarbons such as pyrene are important for ordered packing in these supramolecular architectures.

2.2. Anticancer Activity of Supramolecular Materials of Amphiphiles 1, 2, and 3. Inspired by the enhancement of drug delivery using Neu5Ac-decorated materials,[9,10] the cell viability of HeLa and HEK293 cells was measured in the presence of Neu5Ac-conjugated supramolecular materials to investigate the selectivity and cytotoxicity. The MTT assay results revealed that the vesicles of amphiphile **2** had the highest cytotoxicity to HeLa cells compared with that seen with non-assembled Neu5Ac and materials of amphiphiles **1** and **3** (Figure 4a). In addition, vesicles of **2** showed approximately 30% less cytotoxicity for HEK293 cells compared to HeLa cells, indicating that vesicles of **2** targeted cancer cells more specifically (Figure 4b; see also Figure S15). The MTT assay using compound **S8** that has a pyrene and a tetraethylene glycol linker without Neu5Ac was conducted as a control experiment. Indeed, compound **S8** does not show any selectivity at all, implying that Neu5Ac is essential for targeting cancer cells (Figure 4c).

Cell imaging using a multi-mode reader (cytation) and FOM experiments were performed to compare the relative amount of uptake between ribbons and vesicles *via* the fluorescence of the pyrene group. Each material at 50 μM was used as an optimal concentration in further experiments because vesicles of **2** showed the highest selectivity for HeLa cells at that concentration. The cytation studies corroborated that the uptake of vesicles of **2** was more as the fluorescence intensity in HeLa and HEK293 cells incubated with vesicles of **2** was considerably higher than that of cells incubated with ribbons of **1** (see Figure S16). The results of FOM imaging are consistent with cytation results, showing a strong fluorescence in HeLa cells incubated with vesicles of **2** (see Figure S17).

Pyrene is known to generate ROS, which induces cell death.[25,26] Therefore, we measured the amount of ROS to elucidate the mechanism of cell death due to the presence of the pyrene group. The 2′,7′-dichlorodihydrofluorescein diacetate (DCFDA) assay is a precise technique for directly measuring the ROS in live cells. Non-fluorescent DCFDA is cleaved at two ester bonds by intracellular esterase when it enters the cells, thus leading to the oxidation of the compound into fluorescent 2′,7′-dichlorodihydrofluorescein (DCF) by ROS,[27] which can be detected at 530 nm.[28] The amount of ROS generated is, therefore, proportional to the fluorescence intensity. The HeLa cells incubated with ribbons of **1** did not show any fluorescence, whereas the cells incubated with vesicles of **2** and compound **S8** showed a strong fluorescence of DCF (Figure 4d; see also Figures S18−S20). These results indicated high cytotoxicity in cells after pyrene-induced ROS generation. Overall, the results of the *in vitro* assays indicated that supramolecular materials consisting of Neu5Ac have a higher selectivity for cancer cells (HeLa cells) compared with that for normal cells (HEK293 cells). Among them, vesicles of

https://doi.org/10.1021/acsami.2c02922
ACS Appl. Mater. Interfaces 2022, 14, 16100−16107

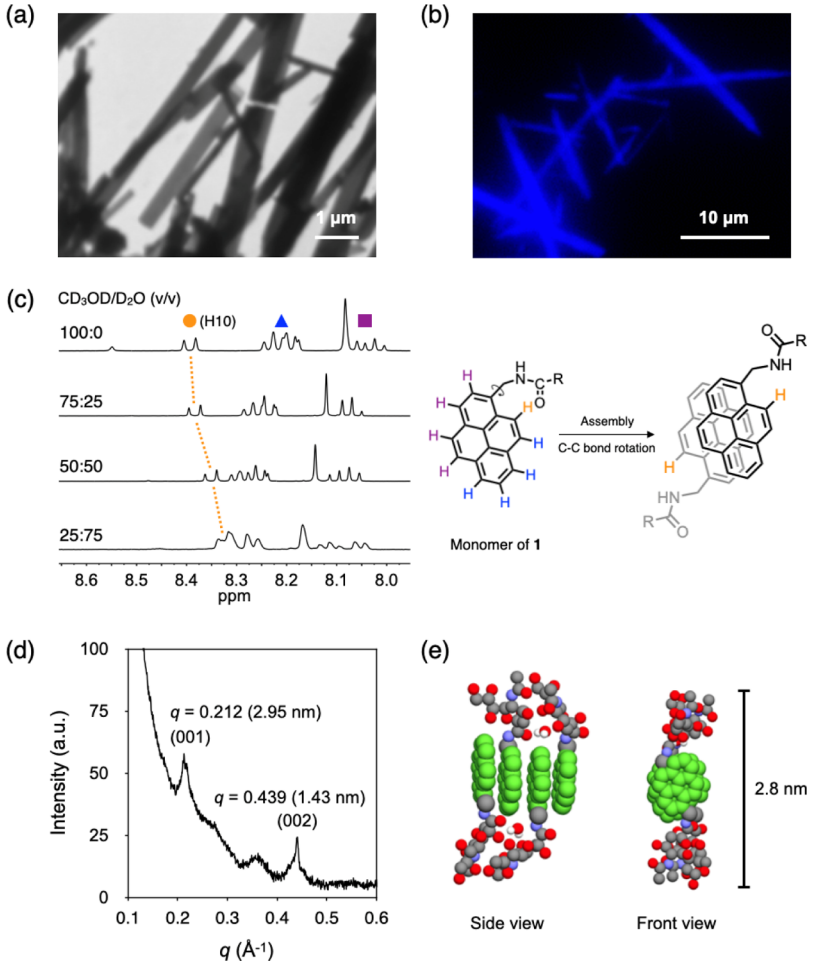

Figure 2. Self-assembled structure of amphiphile **1** in aqueous solution. (a) TEM and (b) FOM images of amphiphile **1** at 200 μM. (c) ^{1}H NMR spectra of amphiphile **1** in CD_3OD/D_2O mixtures with different ratios. The packing arrangement is shown on the *right* side. (d) SAXS result of amphiphile **1**. (e) Molecular simulation of the tetramer of amphiphile **1**.

2 showed a better anticancer activity than that of ribbons of **1** because of their structural feature. Therefore, the selectivity and antitumor effect of supramolecular vesicles can be considered a novel, active-targeting strategy.

3. CONCLUSIONS

Neu5Ac-based pyrene-grafted amphiphiles **1** and **2** and adamantane-grafted amphiphile **3** were synthesized using amide coupling reactions. The amphiphiles **1**, **2**, and **3** in aqueous solution were self-assembled as ribbons, vesicles, and irregular aggregates, respectively, with Neu5Ac exposed on material surfaces. The vesicles of **2** exhibit a remarkable selectivity and a higher uptake ability toward HeLa cells because of the Neu5Ac-coated discrete spherical nanostructures with a smaller size compared to ribbons of **1**. HeLa cells incubated with vesicles of **2** showed the highest fluorescence in the DCFDA assay, implying that the high cytotoxicity is due to ROS generation from the pyrene group. The antitumor effect in HeLa cells by the distinct structural characteristics of vesicle of **2** indicated the relationship between Neu5Ac-conjugated architectures and their anticancer activity. The changing of size in diameter of discrete spherical nanostructures will be performed in the next study to find out the optimal size conditions for the selectivity and antitumor activity for cancer cells. In conclusion, Neu5Ac-conjugated synthetic vesicles using the molecular self-assembly can provide insights into next-generation materials for actively targeting cancer therapy.

4. EXPERIMENTAL SECTION

4.1. General Methods. All starting materials, solvents, and organic reagents were obtained from commercial suppliers (TCI, Aldrich, etc.) and were used without further purification unless otherwise mentioned. Dichloromethane (DCM), *N*,*N*-diisopropylethylamine, and *N*-methylmorpholine (NMM) were dried using distillation from CaH_2. Distilled water (DW) was prepared using ion exchange and filtration. Thin-layer chromatography was performed on precoated glass-backed plates (silica gel 60 F254 0.25 nm), and the components were visualized by observation under ultraviolet light (254 and 365 nm) or by treating the plates with iodine, anisaldehyde, $KMnO_4$, phosphomolybdic acid, and vanillin, followed by heating. The products were purified by flash column chromatography on silica gel (230−400 mesh). Mass spectrometry was performed using an Expression CMS (Advion) electrospray ionization (ESI) mass spectrometer. Analytic and preparatory HPLCs were performed with LC-20AR (Shimadzu) equipped with an YMC-Pack Pro C18 reverse-phase column (250 × 4.6 mm I.D) and a YMC-Actus Triart C18 (250 × 20.0 mm I.D), respectively. ^{1}H and ^{13}C NMR spectra were obtained using a 400 MHz FT-NMR spectrometer using JNM-ECZ400S/L1. All of the absorption and emission spectra were obtained using an Agilent 8453E UV−visible spectrophotometer and a Hitachi F-7000 fluorescence spectrophotometer, respectively. The size of the vesicles was characterized by dynamic light scattering at a fixed angle of θ = 90° using a Nanosight (LM10, Malvern) and

https://doi.org/10.1021/acsami.2c02922
ACS Appl. Mater. Interfaces 2022, 14, 16100−16107

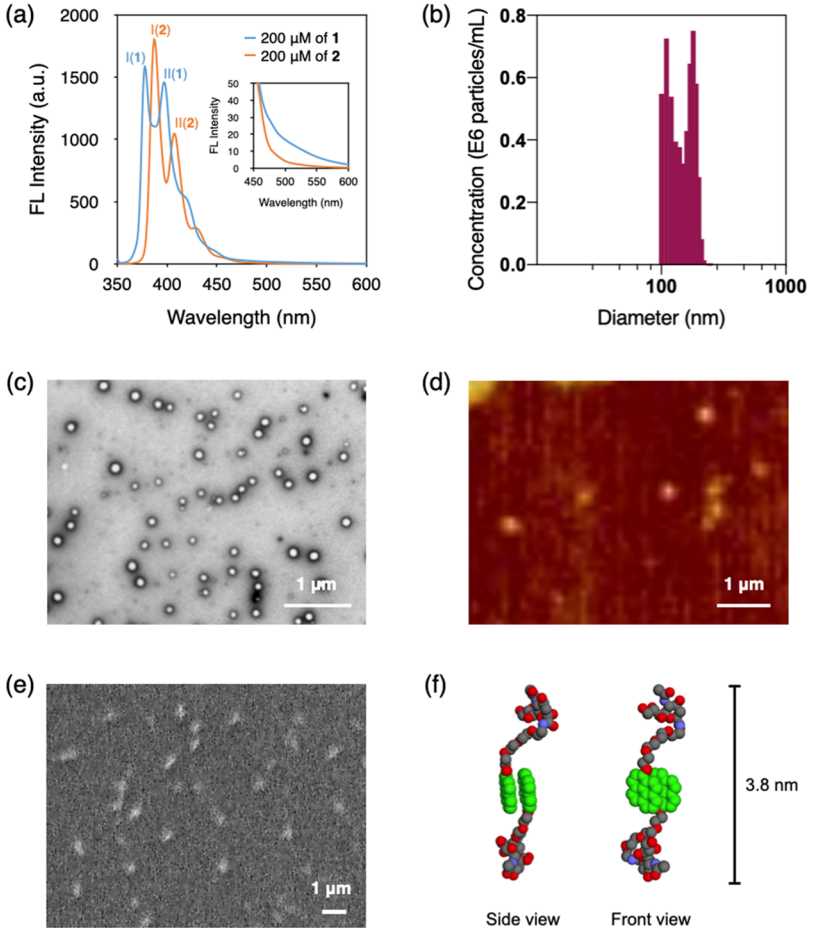

Figure 3. Self-assembled structure of amphiphile **2** in aqueous solution. (a) Emission spectra of amphiphiles **1** and **2** with two intense characteristic peaks I and II of the pyrene fluorophore. Inset are the magnified spectra. (b) Particle size of the self-assembled amphiphile **2** measured by dynamic light scattering. (c) TEM, (d) AFM, and (e) SEM images of vesicles of **2**. (f) Molecular simulation of the packing arrangement in the dimer of amphiphile **2**.

analyzed with NTA 2.3 software. Gel permeation chromatography (GPC) using a Sephadex G-50 (Sigma-Aldrich) was conducted to verify the supramolecular vesicle structure. The microscope slides were cleaned using a traditional piranha solution and cut into small pieces (50 × 50 mm) using a diamond cutter for SEM experiments. Approximately 20 μL of each sample solution was placed on a piece of a microscope slide (25 × 75 mm, ca. 1 mm, Heinz Herenz, Hamburg) by drop-casting and dried under ambient conditions. The sample-loaded microscope slides were coated with Pt (~4 nm) using a Hitachi ion sputter E-1010 and observed using a Hitachi S-4300 under the conditions of 5 kV and 10 μA. X-ray scattering measurements were performed in transmission mode with synchrotron radiation at the 3C X-ray beamline at the Pohang Accelerator Laboratory.

4.2. TEM Experiments. 2 to 4 μL of the sample solution was placed on a carbon-coated grid by drop-casting (Carbon Type B (12–25 nm) on a 200 mesh, with Formvar; Ted Pella, Inc). The solution was evaporated under ambient conditions and then stained by depositing a drop of uranyl acetate aqueous solution (0.4 wt %) on the surface of the sample-loaded grid. The dried specimen was observed using a Hitachi H-7100 and a H-7650 operated at 100 and 80 kV, respectively.

4.3. AFM Experiments. The supramolecular materials were diluted in aqueous solution to investigate the thickness. 20 μL of the sample solutions was drop-cast on mica or an SI wafer and evaporated under ambient conditions. The measurements were subsequently performed using an NX-10 (Park Systems), and the images were acquired in tapping mode.

4.4. Molecular Simulations. Conformer search of *N*-(pyren-1-ylmethyl)acetamide, a truncated structure, was performed using a MacroModel module from Schrödinger Suites (Schrödinger K.K.) with the following parameters; force field: OPLS3, solvent: water, cutoff: none, minimization method: PRCG, maximum iterations: 2500, converge on: gradient, convergence threshold: 0.05, CSearch method: Mixed torsional/low-mode sampling, maximum number of steps: 1000, 100 steps per rotatable bond, energy window for saving structures: 21 kJ/mol, and elimination of redundant conformers using a maximum atom deviation cutoff of 0.5 Å. The resulting eight conformers were optimized, and the NMR chemical shifts of the optimized eight conformers were calculated with a single point structure using the DFT B3LYP-D3 (6-31G**) method using Gaussian 09 software. The optimization of the tetramer of amphiphile **1** was performed using the DFT PBE-D3 (6-31G*) method.

4.5. *In Vitro* Assays. Human cervical cancer cells (HeLa) and HEK293 cells (Korean Cell Line Bank, Seoul, Korea) were cultured in DMEM (HyClone, Logan, UT, USA) supplemented with 10% FBS (Equitech-Bio) and 1% P/S (penicillin/streptomycin, HyClone, Logan, UT, USA). HeLa and HEK293 cells at a density of 1.0 × 10^5 cells/well were seeded in each blank of the well plates, and incubation for all processes was conducted under 37 °C and 5% CO_2 conditions unless otherwise mentioned.

For the cell toxicity test, human cervical cancer cells (HeLa cell) and HEK293 cells were seeded in 96-well plates and incubated for a day with different concentrations of samples. Cells were then washed with phosphate-buffered saline (PBS) and incubated with thiazolyl blue tetrazolium bromide (0.5 mg/mL; Sigma-Aldrich, St. Louis, MO, USA) for 4 h. The medium was discarded, and the generated

https://doi.org/10.1021/acsami.2c02922
ACS Appl. Mater. Interfaces 2022, 14, 16100−16107

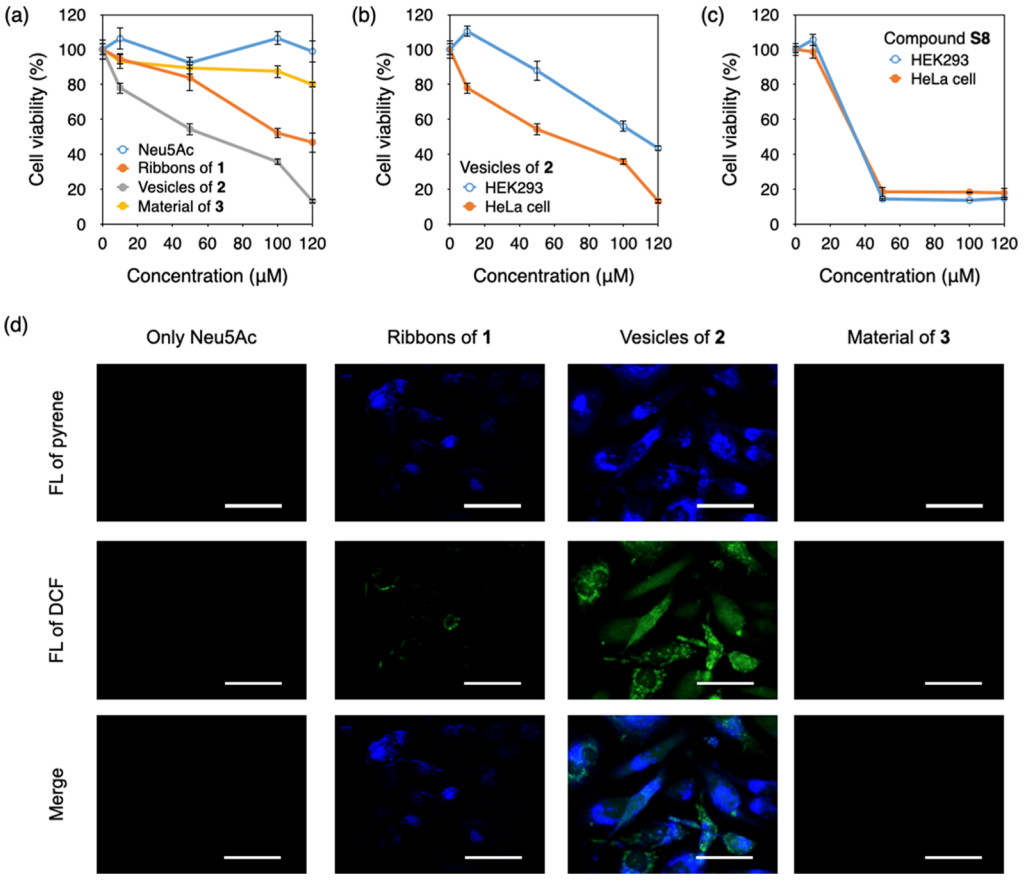

Figure 4. Selectivity and antitumor effect observed in HeLa cells incubated with supramolecular materials compared with those observed in HEK293 cells. (a) Cell viability of HeLa cells incubated with non-assembled Neu5Ac and materials of **1**, **2**, and **3** measured using the MTT assay. (b,c) Cell viability of HeLa and HEK293 cells incubated with (b) vesicles of **2** and (c) compound **S8**. (d) FOM images from the fluorescence DCFDA assays of HeLa cells after incubation with non-assembled Neu5Ac and materials of **1**, **2**, and **3**. The fluorescence details corresponding to the images are marked on the *left* side, and the names of the materials are on the *top* (scale bar, 50 μm).

formazan crystals were dissolved in dimethyl sulfoxide (DMSO) (Sigma-Aldrich). The absorbance was measured at 570 nm (Epoch, Biotec, USA).

For the cell uptake efficiency test, HeLa and HEK293 cells were seeded on black 96-well plates and incubated for 4 h with different concentrations of samples. After replacing the medium, the plates were excited at 342 nm, and the fluorescence intensity was measured at 400 nm (excitation and emission wavelength of pyrene, respectively) using Cytation3 imaging multi-mode readers (BioTek). FOM (Leica DMi8) was also used to confirm cell uptake. Fluorescence of pyrene was observed using an excitation filter at λ_{ex} = 340−380 nm and an emission filter at λ_{em} > 425 nm.

2′,7′-Dichlorofluorescein diacetate (D6883) was purchased from Sigma-Aldrich for the DCFDA assay. HeLa cells with a density of 2.0 × 10^5 cells/well were seeded on a 24-well plate or on a confocal dish and incubated for 24 h. Then, the cells were incubated with each sample for 4 h, and then 300 μL of 50 μM DCFDA was added. After 40 min, the medium was replaced with PBS (pH 7.4), and the fluorescence was observed using FOM. The fluorescence of DCF was observed using an excitation filter at λ_{ex} = 460−500 nm and an emission filter at λ_{em} = 512−542 nm.

4.6. Synthetic Methods. *4.6.1. Synthesis of the Amide Bond (Molecules **1**, **2**, and **3**).* To a solution of Neu5Ac in DMF (0.1 M) were added RNH_2 (1 equiv), NMM (1 equiv), and HATU (1.5 equiv). The reaction was stirred overnight at room temperature. Purification of the mixture using reversed chromatography (H_2O/CH_3CN 95:5 → 0:100 for 30 min) gave the target molecules **1**, **2**, and **3**.

*4.6.2. Synthesis of Hydrophobic Groups of Molecules **1** and **2**.*
*4.6.2.1. Compound **S1**.* Pyrene-1-carboxylic acid (1.0 mmol, 250 mg) was dissolved in 10 mL of dry tetrahydrofuran (THF) and cooled to 0 °C. Then, 125 μL of lithium aluminum hydride (2.4 M in THF) was added dropwise, and the reaction was stirred for 4 h. The reaction was quenched slowly with DW, and DCM was added. The organic phase was washed with brine and dried with $MgSO_4$ and filtered. The mixture was then loaded on a silica-gel column chromatograph (ethyl acetate/hexane 1:2) to afford compound **S1** as a yellow powder in 77% yield (180 mg). ^{1}H NMR (400 MHz, $CDCl_3$, δ): 8.48−7.92 (m, 9H), 5.43 (d, 2H, J = 4.7 Hz), 1.85 (t, 1H, J = 5.5 Hz).

*4.6.2.2. Compound **S2**.* Compound **S1** (0.56 mmol, 130 mg) was suspended in toluene and cooled to 0 °C. Then, 100 μL of phosphorus tribromide was added dropwise, and the reaction was stirred for 2 h under Ar in the dark. The resulting solution was neutralized with saturated $NaHCO_3$ aq. and extracted with toluene. The organic layer was washed with brine and dried over anhydrous $MgSO_4$. Evaporation of the solvent *in vacuo* afforded compound **S2** as a yellow powder in 71% yield (117 mg). ^{1}H NMR (400 MHz, $CDCl_3$, δ): 8.42−8.02 (m, 9H), 5.2 (s, 2H).

*4.6.2.3. Compound **S3**.* Compound **S2** (0.40 mmol, 117 mg) was suspended in 4 mL of dry acetonitrile and heated to 50 °C. Then, 140 mg of sodium azide was added, and the reaction was stirred for 2 h. The resulting solution was quenched with brine and extracted with ethyl acetate. The organic layer was dried over anhydrous $MgSO_4$. The mixture was then loaded on a silica-gel column chromatograph (ethyl acetate/hexane 1:10) to afford compound **S3** as a green powder in 92% yield (95 mg). ^{1}H NMR (400 MHz, $CDCl_3$, δ): 8.37−7.91 (m, 9H), 5.05 (s, 2H).

*4.6.2.4. Compound **S4**.* To a solution of **S3** (0.40 mmol, 95 mg) in a mixture of ethanol/THF 1:1 (2 mL) was added palladium 10% on carbon (w/w 1:2, 190 mg) under a H_2 atmosphere and stirred for 2 h

https://doi.org/10.1021/acsami.2c02922
ACS Appl. Mater. Interfaces 2022, 14, 16100−16107

at room temperature. The resulting solution was diluted with ethanol and filtered. Evaporation of the solvent *in vacuo* afforded compound **S4** as an orange syrup in 89% yield (76 mg). ^{1}H NMR (400 MHz, $CDCl_3$, δ): 8.43−7.94 (m, 9H), 4.59 (s, 2H).

*4.6.2.5. Compound **S5**.* To a solution of tetraethylene glycol (0.5 mmol, 90 μL) in DCM (1.5 mL) were added tosyl chloride (1.1 mmol, 200 mg) and potassium hydroxide (8 mmol, 230 mg) slowly. The reaction was stirred at 0 °C for 3 h. The mixture was quenched slowly with DW and extracted with DCM. The organic phase was washed with brine and dried with $MgSO_4$ and filtered. The mixture was then loaded on a silica-gel column chromatograph (ethyl acetate/hexane 1:5 → 10:0) to afford compound **S5** as a yellow syrup in 80% yield (206 mg). ^{1}H NMR (400 MHz, $CDCl_3$, δ): 7.79 (d, J = 8.4 Hz, 4H), 7.34 (d, J = 7.9 Hz, 4H), 4.17−4.13 (m, 4H), 3.70−3.66 (m, 4H), 3.56 (q, J = 1.2 Hz, 8H), 2.44 (s, 6H); ESI-MS m/z: $[M + 2Na - H]^+$ calcd for $C_{22}H_{30}Na_2O_9S_2$, 547.1; found, 547.1.

*4.6.2.6. Compound **S6**.* To a solution of compound **S5** (0.4 mmol, 206 mg) in CH_3CN (2.5 mL) was added sodium azide (0.4 mmol, 26.0 mg), and the mixture was refluxed at 80 °C overnight. The mixture was quenched with brine and extracted with ethyl acetate. The organic phase was dried with $MgSO_4$ and filtered. The mixture was then loaded on a silica-gel column chromatograph (ethyl acetate/hexane 2:1) to afford compound **S6** as a yellow syrup in 38% yield (58 mg). ^{1}H NMR (400 MHz, $CDCl_3$, δ): 7.80 (d, J = 8.3 Hz, 2H), 7.34 (d, J = 8.3 Hz, 2H), 4.20−4.13 (m, 2H), 3.71−3.59 (m, 4H), 3.39 (q, J = 4.8 Hz, 8H), 2.45 (s, 3H), 1.68 (d, J = 0.9 Hz, 2H); ESI-MS m/z: $[M + H]^+$ calcd for $C_{15}H_{23}N_3O_6S$, 374.1; found, 373.9, $[M + Na]^+$ calcd for $C_{15}H_{23}N_3NaO_6S$, 396.1; found, 396.5.

*4.6.2.7. Compound **S7**.* To a solution of compound **S6** (0.16 mmol, 58 mg) in CH_3CN (1.5 mL) were added 1-hydroxypyrene (0.16 mmol, 34 mg) and cesium carbonate (1.5 mmol, 490 mg) under Ar, and the mixture was refluxed at 80 °C overnight. The mixture was then quenched slowly with DW and extracted with ethyl acetate. The organic phase was washed with brine and dried with $MgSO_4$ and filtered. The mixture was then loaded on a silica-gel column chromatograph (ethyl acetate/hexane 1:1) to afford compound **S7** as a yellow syrup in 50% yield (33 mg). ^{1}H NMR (400 MHz, $CDCl_3$, δ): 8.51−7.53 (m, 9H), 4.52−4.47 (m, 2H), 4.09−4.06 (m, 2H), 3.86−3.83 (m, 2H), 3.75−3.72 (m, 2H), 3.70−3.67 (m, 2H), 3.65−3.60 (m, 4H), 3.32 (dd, J = 5.6, 4.6 Hz, 2H); ESI-MS m/z: $[M + Na]^+$ calcd for $C_{24}H_{25}N_3NaO_4$, 442.17; found, 442.6.

*4.6.2.8. Compound **S8**.* To a solution of compound **S7** (0.078 mmol, 33 mg) in THF (0.16 mL) were added ethanol anhydride (0.2 mL) and palladium 10% on carbon (0.5 w/w, 16.4 mg) under H_2, and the mixture was stirred overnight at room temperature. The mixture was then filtered using a syringe filter to afford compound **S8** as a yellow syrup in 41% yield (12.6 mg). ^{1}H NMR (400 MHz, $CDCl_3$, δ): 8.50−7.53 (m, 9H), 4.53−4.49 (m, 2H), 4.08 (dd, J = 5.5, 4.2 Hz, 2H), 3.90−3.80 (m, 2H), 3.74 (dd, J = 5.8, 3.8 Hz, 2H), 3.68 (dd, J = 5.9, 3.4 Hz, 2H), 3.62 (dd, J = 5.5, 4.2 Hz, 2H), 3.54−3.46 (m, 2H), 2.78 (dt, J = 31.9, 5.4 Hz, 2H); ESI-MS m/z: $[M + H]^+$ calcd for $C_{24}H_{28}NO_4$, 394.49; found, 394.2.

4.7. Preparation of Supramolecular Materials. Molecules **1**, **2**, and **3** were fully dried in high *vacuo*, and a portion of the products were diluted to make a stock solution of 0.1 wt % in methanol/H_2O 7:3. Then, a required amount for samples with different concentration was taken from the stock solution and put into another vial and evaporated. An appropriate amount of solvent for self-assembly was added according to the targeting concentration and sonicated for 30 min under ambient conditions. All the samples were incubated in the dark at room temperature until the supramolecular structures were stabilized.

■ ASSOCIATED CONTENT

Supporting Information

The Supporting Information is available free of charge at https://pubs.acs.org/doi/10.1021/acsami.2c02922.

Molecular mass and analytic HPLC spectra for molecules **1**, **2**, and **3**; ^{1}H and ^{13}C NMR spectra of molecules **1**, **2**, and **3**; absorption and emission spectra of molecules **1** and **2** at different concentrations; AFM image of amphiphile **1** at 200 μM; SEM image of amphiphile **1** at 200 μM; DFT-based proton NMR prediction of *N*-(1-pyrenylmethyl)acetamide; molecular simulation of dimers **1** and **2**; FOM image of spherical structures of molecule **2** at 140 μM; encapsulation of pyranine into the vesicles; SAXS spectrum of molecule **2**; self-assembled structure of amphiphile **3** in an aqueous solution; cell viability of HeLa and HEK293 cells measured using the MTT assay; fluorescence intensity of HeLa and HEK293 measured using cytation at 400 nm; TEM images of only Neu5Ac or materials of **1**, **2**, and **3** and FOM images of those incubated with HeLa and HEK293 cells; fluorescence intensity of DCFDA-dyed HeLa cells measured by FOM images; FOM images of HeLa cells dyed with DCFDA to confirm the amount of intracellular ROS generated by the pyrene group; and FOM images of HeLa cells without the DCFDA dye (PDF)

■ AUTHOR INFORMATION

Corresponding Author

Yongju Kim − *KU-KIST Graduate School of Converging Science and Technology, Department of Integrative Energy Engineering, Korea University, Seoul 02841, Republic of Korea;* orcid.org/0000-0002-5862-5228; Email: yongjukim@korea.ac.kr

Authors

Jiwon Hwang − *KU-KIST Graduate School of Converging Science and Technology, Department of Integrative Energy Engineering, Korea University, Seoul 02841, Republic of Korea*

Ye Rim Kim − *KU-KIST Graduate School of Converging Science and Technology, Department of Integrative Energy Engineering, Korea University, Seoul 02841, Republic of Korea*

Jung Yeon Park − *KU-KIST Graduate School of Converging Science and Technology, Department of Integrative Energy Engineering, Korea University, Seoul 02841, Republic of Korea*

Woo Hyun Nam − *KU-KIST Graduate School of Converging Science and Technology, Department of Integrative Energy Engineering, Korea University, Seoul 02841, Republic of Korea*

Jehan Kim − *Pohang Accelerator Laboratory, Postech, Gyeongbuk 790-784, Republic of Korea*

Jinhan Cho − *KU-KIST Graduate School of Converging Science and Technology, Department of Chemical and Biological Engineering, Korea University, Seoul 02841, Republic of Korea;* orcid.org/0000-0002-7097-5968

Complete contact information is available at: https://pubs.acs.org/10.1021/acsami.2c02922

Author Contributions

J.H. synthesized the molecules and collected and analyzed all the data. Y.R.K. carried out the *in vitro* experiments. J.Y.P. conducted the TEM experiments. W.H.N. synthesized molecule **1**. J.K. performed the X-ray experiments. Y.K. developed the concept, supervised the research, and wrote the manuscript with input from all authors.

Notes

The authors declare no competing financial interest.

■ ACKNOWLEDGMENTS

This work was supported by the National Research Foundation of Korea (NRF-2019R1C1C1008526 and NRF-2019R1A4A1027627), a Korea University grant, and the KU-KIST School Project.

■ ABBREVIATIONS

SA, sialic acid
Neu5Ac, *N*-acetylneuraminic acid
ROS, reactive oxygen species
TEM, transmission electron microscopy
FOM, fluorescence optical microscopy
AFM, atomic force microscopy
SEM, scanning electron microscopy
NMR, nuclear magnetic resonance
DFT, density functional theory
SAXS, small-angle X-ray scattering
DCFDA, 2′,7′-dichlorodihydrofluorescein diacetate
DCF, 2′,7′-dichlorodihydrofluorescein

■ REFERENCES

(1) Büll, C.; den Brok, M. H.; Adema, G. J. Sweet Escape: Sialic Acids in Tumor Immune Evasion. *Biochim. Biophys. Acta, Rev. Cancer* **2014**, *1846*, 238−246.
(2) Chen, X.; Varki, A. Advances in the Biology and Chemistry of Sialic Acids. *ACS Chem. Biol.* **2010**, *5*, 163−176.
(3) Li, Y.; Chen, X. Sialic acid metabolism and sialyltransferases: natural functions and applications. *Appl. Microbiol. Biotechnol.* **2012**, *94*, 887−905.
(4) Murrey, H. E.; Hsieh-Wilson, L. C. The Chemical Neurobiology of Carbohydrates. *Chem. Rev.* **2008**, *108*, 1708−1731.
(5) Bondioli, L.; Ruozi, B.; Belletti, D.; Forni, F.; Vandelli, M. A.; Tosi, G. Sialic Acid as a Potential Approach for the Protection and Targeting of Nanocarriers. *Expert Opin. Drug Delivery* **2011**, *8*, 921−937.
(6) Yang, H.; Lu, L.; Chen, X. An Overview and Future Prospects of Sialic Acids. *Biotechnol. Adv.* **2021**, *46*, 107678.
(7) Aoki, Y.; Tanimoto, S.; Takahashi, D.; Toshima, K. Photodegradation and inhibition of drug-resistant influenza virus neuraminidase using anthraquinone-sialic acid hybrids. *Chem. Commun.* **2013**, *49*, 1169.
(8) Zheng, J.-S.; Zheng, S.-Y.; Zhang, Y.-B.; Yu, B.; Zheng, W.; Yang, F.; Chen, T. Sialic Acid Surface Decoration Enhances Cellular Uptake and Apoptosis-Inducing Activity of Selenium Nanoparticles. *Colloids Surf., B* **2011**, *83*, 183−187.
(9) She, Z.; Zhang, T.; Wang, X.; Li, X.; Song, Y.; Cheng, X.; Huang, Z.; Deng, Y. The anticancer efficacy of pixantrone-loaded liposomes decorated with sialic acid-octadecylamine conjugate. *Biomaterials* **2014**, *35*, 5216−5225.
(10) Weïwer, M.; Chen, C.-C.; Kemp, M. M.; Linhardt, R. J. Synthesis and Biological Evaluation of Non-Hydrolyzable 1,2,3-Triazole-Linked Sialic Acid Derivatives as Neuraminidase Inhibitors. *Eur. J. Org. Chem.* **2009**, *2009*, 2611−2620.
(11) Jayant, S.; Khandare, J. J.; Wang, Y.; Singh, A. P.; Vorsa, N.; Minko, T. Targeted Sialic Acid-Doxorubicin Prodrugs for Intracellular Delivery and Cancer Treatment. *Pharm. Res.* **2007**, *24*, 2120−2130.
(12) Webber, M. J.; Appel, E. A.; Meijer, E. W.; Langer, R. Supramolecular Biomaterials. *Nat. Mater.* **2016**, *15*, 13−26.
(13) Savyasachi, A. J.; Kotova, O.; Shanmugaraju, S.; Bradberry, S. J.; Ó'Máille, G. M.; Gunnlaugsson, T. Supramolecular Chemistry: A Toolkit for Soft Functional Materials and Organic Particles. *Chem* **2017**, *3*, 764−811.
(14) Sarkar, B.; O'Leary, L. E. R.; Hartgerink, J. D. Self-Assembly of Fiber-Forming Collagen Mimetic Peptides Controlled by Triple-Helical Nucleation. *J. Am. Chem. Soc.* **2014**, *136*, 14417−14424.
(15) Huang, L.; Zhang, H.; Wu, S.; Xu, X.; Zhang, L.; Ji, H.; He, L.; Qian, Y.; Wang, Z.; Chen, Y.; Shen, J.; Mao, Z.-W.; Huang, Z. Charge Regulation of Self-Assembled Tubules by Protonation for Efficiently Selective and Controlled Drug Delivery. *iScience* **2019**, *19*, 224−231.
(16) Shen, B.; Zhu, Y.; Kim, Y.; Zhou, X.; Sun, H.; Lu, Z.; Lee, M. Autonomous Helical Propagation of Active Toroids with Mechanical Action. *Nat. Commun.* **2019**, *10*, 1080.
(17) Shen, B.; He, Y.; Kim, Y.; Wang, Y.; Lee, M. Spontaneous Capture of Carbohydrate Guests Through Folding and Zipping of Self-Assembled Ribbons. *Angew. Chem., Int. Ed.* **2016**, *55*, 2382−2386.
(18) Krishnan, N.; Perumal, D.; Atchimnaidu, S.; Harikrishnan, K. S.; Golla, M.; Kumar, N. M.; Kalathil, J.; Krishna, J.; Vijayan, D. K.; Varghese, R. Galactose-Grafted 2D Nanosheets from the Self-Assembly of Amphiphilic Janus Dendrimers for the Capture and Agglutination of Escherichia coli. *Chem.—Eur. J.* **2020**, *26*, 1037−1041.
(19) Liu, Y.; Wang, H.; Li, S.; Chen, C.; Xu, L.; Huang, P.; Liu, F.; Su, Y.; Qi, M.; Yu, C.; Zhou, Y. In Situ Supramolecular Polymerization-Enhanced Self-Assembly of Polymer Vesicles for Highly Efficient Photothermal Therapy. *Nat. Commun.* **2020**, *11*, 1724.
(20) Marson, D.; Laurini, E.; Aulic, S.; Fermeglia, M.; Pricl, S. Perceptions and Misconceptions in Molecular Recognition: Key Factors in Self-Assembling Multivalent (SAMul) Ligands/Polyanions Selectivity. *Molecules* **2020**, *25*, 1003.
(21) Kim, T.; Park, J. Y.; Hwang, J.; Seo, G.; Kim, Y. Supramolecular Two-Dimensional Systems and Their Biological Applications. *Adv. Mater.* **2020**, *32*, 2002405.
(22) Niu, D.; Jiang, Y.; Ji, L.; Ouyang, G.; Liu, M. Self-Assembly through Coordination and π-Stacking: Controlled Switching of Circularly Polarized Luminescence. *Angew. Chem., Int. Ed.* **2019**, *58*, 5946−5950.
(23) Mohr, A.; Talbiersky, P.; Korth, H.-G.; Sustmann, R.; Boese, R.; Bläser, D.; Rehage, H. A New Pyrene-Based Fluorescent Probe for the Determination of Critical Micelle Concentrations. *J. Phys. Chem. B* **2007**, *111*, 12985−12992.
(24) Philip, S.; Kuriakose, S. Aggregation Enhanced Excimer Emission Supported, Monomeric Fluorescence Quenching of Dendritic Hyperbranched Polyglycerol Coupled 1-Pyrene Butyric Acid Lumophore as a Sensing Probe for Fe_2O_3 Nanoparticles. *J. Fluoresc.* **2019**, *29*, 387−398.
(25) Ma, J.-K.; Saad Eldin, W. F.; El-Ghareeb, W. R.; Elhelaly, A. E.; Khedr, M. H. E.; Li, X.; Huang, X.-C. Effects of Pyrene on Human Liver HepG2 Cells: Cytotoxicity, Oxidative Stress, and Transcriptomic Changes in Xenobiotic Metabolizing Enzymes and Inflammatory Markers with Protection Trial Using Lycopene. *BioMed Res. Int.* **2019**, *2019*, 7604851.
(26) Yin, Y.; Jia, J.; Guo, H. Y.; Yang, L. Y.; Wang, X. R.; Sun, Y. Y. Pyrene-stimulated reactive oxygen species generation and oxidative damage inCarassius auratus. *J. Environ. Sci. Health, Part A: Toxic/Hazard. Subst. Environ. Eng.* **2014**, *49*, 162−170.
(27) Eruslanov, E.; Kusmartsev, S. Advanced Protocols in Oxidative Stress II. *Methods in Molecular Biology (Methods and Protocols)*; Armstrong, D., Ed.; Humana Press: Totowa, NJ, 2010; Vol. *594*, pp. 60−62.
(28) Pogue, A. I.; Jones, B. M.; Bhattacharjee, S.; Percy, M. E.; Zhao, Y.; Lukiw, W. J. Metal-Sulfate Induced Generation of ROS in Human Brain Cells: Detection Using an Isomeric Mixture of 5- and 6-Carboxy-2′,7′-Dichlorofluorescein Diacetate (Carboxy-DCFDA) as a Cell Permeant Tracer. *Int. J. Mol. Sci.* **2012**, *13*, 9615−9626.

https://doi.org/10.1021/acsami.2c02922
ACS Appl. Mater. Interfaces 2022, 14, 16100−16107